

Correction of scatter in computed tomography images of bone

T. N. Hangartner^{a)}

Department of Applied Sciences in Medicine, The University of Alberta, Edmonton, Canada T6G 2G3

(Received 13 August 1986; accepted for publication 11 March 1987)

A cylindrical aluminum/Plexiglas phantom representing trabecular bone surrounded by various amounts of cortical bone was constructed. Measurements of this phantom using a computed tomography scanner with a ^{125}I photon source demonstrated errors of 0% to 28% in the density of trabecular bone. Two contributing factors are identified: scatter and exponential edge-gradient effect. A simple first-order correction is developed to correct for the scatter-induced error. Relative to the exponential edge-gradient effect, which contributes up to 3.4% error over the range of cortical thicknesses measured, the correction procedure reduces the scatter-induced error to a level of -0.66% to $+0.61\%$. The consistency of the optimized correction parameters with the physical model as well as the effect of scatter measured by the same phantom on a GE 8800 scanner are shown.

Key words: computed tomography, scatter, bone measurements

I. INTRODUCTION

In calculating projection values in computed tomography (CT) images it is assumed that photons are removed from the measured beam after their first interaction with material in the beam path. This results in a linear density scale (e.g., Hounsfield units) proportional to the coefficients of linear attenuation in the reconstructed image. However, coherent and incoherent scattering changes the pathway of some photons, and these may scatter into neighboring detectors. The fraction of scattered photons seen by a detector depends upon the energy of the incident beam, the type of material in the beam path, the detector's energy-selection capability, and the collimation geometry of both source and detector. Beam energy and object composition are largely fixed, and energy selection and collimators can be optimized for a particular system. This led to the fact that most published data about scatter assume a round water phantom,¹⁻³ and proposed scatter corrections are independent of the measurement object.^{4,5} However, whereas detected scattered photons might degrade the visual impression of the final image only minimally, particularly if density varies little in the measured cross section, inhomogeneities of high density (e.g., bone) produce streaks. Large inhomogeneities alter the reconstructed values inside the high-density structure and in neighboring low-density areas. Although streaks can be minimized with corrections that take scatter as a constant fraction of the unattenuated photon intensity into account,^{4,5} quantitative analysis of the values still reveals errors of several percent.

The author's current objective is the quantitative assessment of trabecular bone density. Several investigators have addressed the problem of accuracy in single- and dual-energy CT measurements in the spine, predominantly in the context of variable fat content of the bone marrow.⁶⁻⁸ In the present study, the influence of variation in the amount of surrounding cortical bone on the measured density values of trabecular bone is investigated. Two contributing factors, photon scattering and exponential edge-gradient (EEG) ef-

fect, are identified, and a correction method for the error produced by scatter is developed and tested.

II. EXPERIMENTS

Variation in the amount of cortical bone was simulated in a phantom consisting of a Plexiglas cylinder with an aluminum insert of five wall thicknesses (Fig. 1). The outer space was filled with water, representing soft tissue, and the inner space with a solution of K_2HPO_4 in water (150 mg/ml) to simulate trabecular bone with marrow.

The phantom was measured at each wall thickness on a γ -CT scanner (Fig. 2) that uses a ^{125}I source with an average energy of about 29 keV.⁹ The measurement for an aluminum-wall thickness of zero was carried out with an insert of Plexiglas with 0.3 mm wall thickness. The region of interest for averaging trabecular bone values was a central circle, 14.4-mm diameter, sufficiently distant from the inner aluminum edge to avoid its direct influence on the CT values. For these measurements, our normal analytical beam hardening correction was performed. This involves the measurement of about 20 sandwiched plates of 5.8 mm Plexiglas and 0.8 mm aluminum. The measured projection values (natural log of count rate through air divided by count rate through stack of plates) are plotted as y values against the number of plates in each stack as x values. A second degree polynomial is fitted

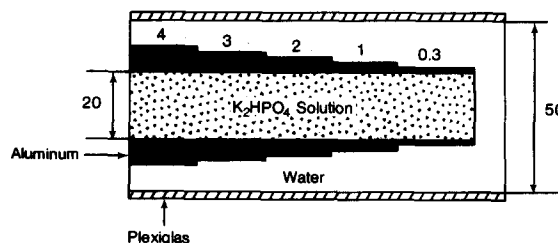


FIG. 1. Section through the cylindrical phantom used to demonstrate the influence of scatter on the reconstructed value of a solution of 150 mg/ml K_2HPO_4 in water. Dimensions in mm.

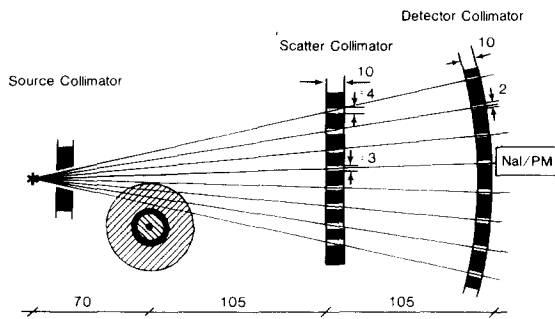


FIG. 2. Geometry of translate-rotate scanner with fixed source and detector collimators and adjustable scatter collimator (dimensions in mm). The openings in the scatter collimator are made as narrow as possible in the imaging plane to minimize scatter without reducing the intensity of the primary beam. The opening of the collimators in z direction is 1 mm for the source collimator and 5 mm for the scatter and detector collimators.

through these points, representing the calibration curve. A mono-energetic radiation beam would produce a straight line, but poly-energetic beams cause the curve to show a reduced slope towards higher absorber thicknesses. The correction procedure now replaces a measured projection value of a CT image with the appropriate value of the straight line at the same x value. Increasing thickness of the walls was paralleled by increasing density values inside the aluminum ring (Fig. 3). Curves are given for measurements with and without a scatter collimator in front of the detector collimators. The measured density changes of the center solution are caused by the following factors.

Water is an excellent scatterer, and the fan beam (2nd-

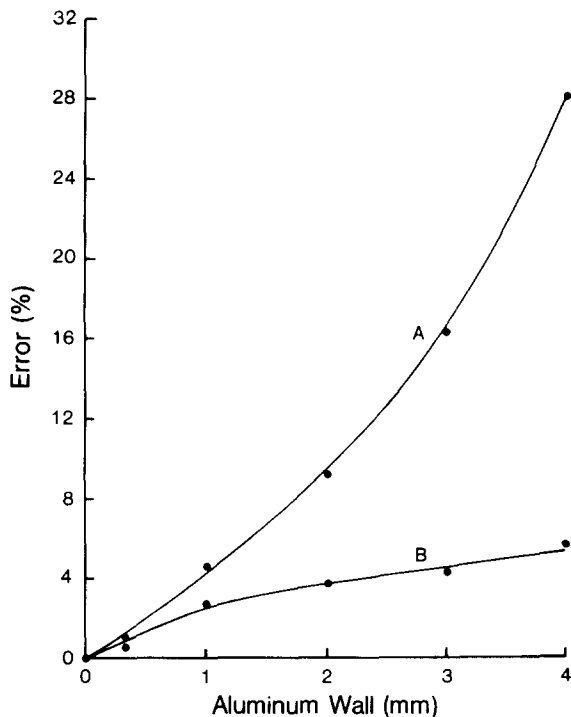


FIG. 3. Relative error of the linear attenuation coefficients of the K_2HPO_4 solution surrounded by aluminum rings of varied wall thicknesses, measured by γ -CT. Curve A was obtained without the scatter collimator, curve B with the scatter collimator in place.

generation system) used with the scanner irradiates a wide section of the phantom at any one time. For a detector measuring photons along a beam path through the aluminum, a certain amount of scatter from the surrounding water elevates the measured count rate and makes the amount of aluminum in the projection value appear smaller than it should be. We used a convolution/backprojection algorithm to reconstruct the images¹⁰; this reverses the error for points that are further from the high-density structure, largely because the convolution kernel contains a positive value in the center and negative weighting factors to the left and right. As a result, the values subtracted for aluminum at points some distances from the ring are smaller than they should be, thereby increasing both the total sum and the backprojected density values.

Physical measurement of the amount of scatter was performed with the primary beam to a particular detector occluded by positioning a piece of lead in front of the scatter collimator. The scatter-to-primary ratio of a photon beam crossing the phantom in proximity of the aluminum insert, but still completely in the outer water-filled compartment, was in the average 5.7×10^{-3} for the setup without the scatter collimator and 7.4×10^{-5} with the scatter collimator in place. This ratio changed by less than $\pm 25\%$ for the various aluminum-wall thicknesses and is in the same order of magnitude as the one measured for a large 48-mm-thick Plexiglas plate (6.2×10^{-3} and 30×10^{-5} , respectively). Although the number of scattered photons increases towards the edge of the phantom and then decreases when the fan beam leaves the object, the scatter-to-primary ratio constantly decreases. This is consistent with scatter measurements published by Johns and Yaffe.¹

The phantom used for studying the effect of scattering represents a worst-case situation. Nevertheless, it reflects the geometry and density distribution of long bones. Scattering, being a systematic error, degrades the accuracy of bone-density measurements. As the scatter measurements show a reduction of scattered photons in the center of the phantom by a factor of 2 to 5, an object-independent correction that assumes scatter to be a constant fraction of the incident photon flux^{4,5} is likely not to be an optimal correction. We attempted, therefore, to develop a scatter correction which takes the material distribution of the object into account and which can easily be implemented in the reconstruction process without using iterative methods. Such a correction method can necessarily include estimates only for first-order scattering.

III. SCATTER CORRECTION METHOD

In developing an estimate of the fractional amount of scattered photons, let us assume a photon beam of intensity I_0 traversing a homogeneous object of thickness a_0 (Fig. 4). The intensity of photons entering the volume element of thickness da is

$$I_a = I_0 e^{-\mu a}, \quad (1)$$

where μ = linear attenuation coefficient of the material in the beam path and a = length of beam path from entry point to volume element. If μ_s denotes the combined coefficient of

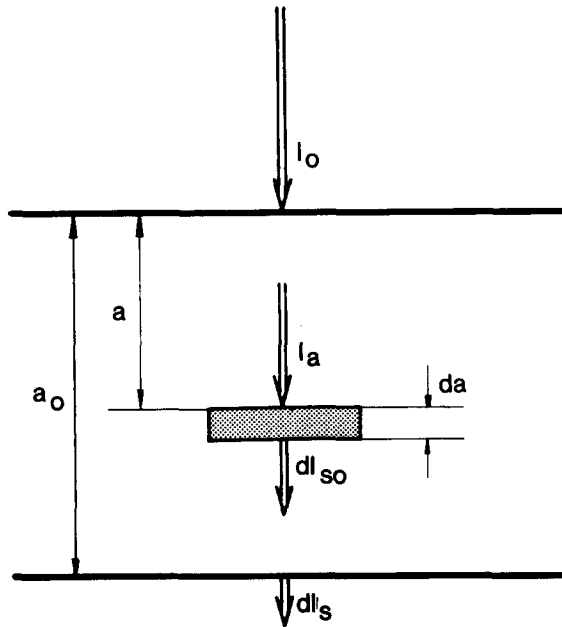


FIG. 4. Definition of parameters used for developing the correction of scatter.

coherent and incoherent scattering, the intensity of scattered photons (dI_{S0}) from the volume element with thickness da is

$$dI_{S0} = I_a \mu_S da. \quad (2)$$

Only the fraction f of all the scattered photons is scattered forwards. These forward-scattered photons are attenuated, so that the intensity of observed scattered photons (dI_S) from this volume element is

$$dI_S = f dI_{S0} e^{-\mu(a_0 - a)}. \quad (3)$$

Combining Eqs. (1)–(3), we obtain

$$dI_S = f I_0 e^{-\mu a} \mu_S da e^{-\mu(a_0 - a)}. \quad (4)$$

This considers only first-order scattering. We have assumed that the forward-scattered photons have similar energy as the incident photons, and we therefore use the same μ value for incident and for scattered photons.

The intensity of all forward-scattered photons (I_S) is the integral of Eq. (4) over the thickness of the object

$$I_S = \int_0^{a_0} dI_S = I_0 f \mu_S e^{-\mu a_0} a_0. \quad (5)$$

The length of the beam path through the object (a_0) can be estimated by replacing a with a_0 in Eq. (1):

$$a_0 = 1/\mu \ln(I_0/I), \quad (6)$$

where I = beam intensity attenuated by object of thickness a_0 . Substituting a_0 in Eq. (5) yields

$$I_S = f (\mu_S/\mu) I \ln(I_0/I) \quad (7)$$

or

$$I_S = p I \ln(I_0/I), \quad (8)$$

p being a material- and energy-specific constant. Assuming I_S is small compared with I , the measured count rates can be used to estimate $I \ln(I_0/I)$. The variable p contains the fraction of forward-scattered photons and the ratio of scatter cross section to attenuation cross section. The two major

materials in the cross sections are bone and soft tissue. The ratio of μ_S/μ at 30 keV for bone^{11,12} is 0.20, for soft tissue 0.60. If f is assumed to be independent of the type of tissue, p changes with the relative amounts of bone and soft tissue in the beam path according to the change in μ_S/μ . Approximate values for the tissue distribution would have to be obtained from a preliminary reconstruction of the measured cross section. However, this leads to an iterative procedure of scatter correction and will not be discussed here. We will assume p to be a universal constant that is experimentally defined such that the error due to scatter in the measured phantom is minimized.

So far our calculations have been based only on forward-scattered photons. However, the collimators in front of the detectors allow photons from a certain angle off the centerline to be seen by the detector. Analysis of the geometry of the scatter collimator reveals that the scatter acceptance angle of the detectors is 2.73° . This translates into a width of 8.0 mm at the center of rotation or $n = 27$ projection points (out of 256). For this narrow forward angle we can assume isotropic distribution of the scattered photons and a minimal shift in energy; we therefore apply the same attenuation coefficients as for the forward-scattered photons. The scatter acceptance angle is taken into account by summing the expression for forward-scattered photons [Eq. (8)] over the scatter acceptance angle (i.e., n points) and assigning the sum to the center value. As the collimators define a specific angular sensitivity function for the detectors, the n scatter values are weighted with that function before the summation is carried out. Based on the arrangement of the detector and scatter collimators, the sensitivity function has a trapezoidal shape with a base of 27 data points and a centered top of 13 data points. The sensitivity in the center of the trapezoid is one and decreases linearly on both sides to zero. In practice, slight variations in the sensitivity function may be necessary in order to minimize the scattering error in the calibration phantom. It was found that the shape of the sensitivity function is not very critical and can be replaced with a function of equal weights but smaller width without introducing major changes in the resultant images.

The question remains: How much can the error of the K_2HPO_4 solutions be reduced? Because the projection data are obtained from measured attenuations of a photon beam of finite width, inhomogeneities in the cross section lead to the EEG effect.¹³ Mathematical simulations of the measured phantom cross sections, that take into account the energy spectrum of the ^{125}I source and the beamwidth of the scanner, but not the scattering contribution, reveal an error of up to 3.4% for the K_2HPO_4 solution. Therefore, optimization of the parameters p and n should correct for only the scattering-induced error, and not for errors due to the EEG effect.

IV. RESULTS

Measurements of the previously described phantom were obtained at each of the various aluminum-wall thicknesses. For a wall thickness of 0 mm aluminum, the aluminum insert was replaced with a Plexiglas insert of 0.3 mm wall thickness and also measured with and without the scatter collimator mounted. The parameters p and n were varied for

each of the two measurement series separately. For a given pair of p and n , the average reconstructed value of the K_2HPO_4 solution in each cross section was computed. These values were compared with the values due to the EEG effect, and the sum of the squared differences was calculated. The pair of p and n with the smallest sum of squared differences was selected as the optimal set of correction parameters, and the curves produced by these sets are shown in Fig. 5. The corrected values represent the total remaining error which is

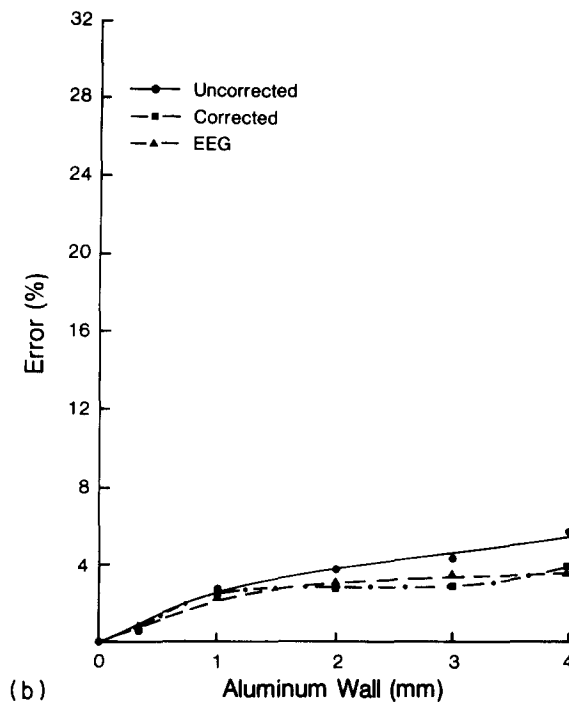
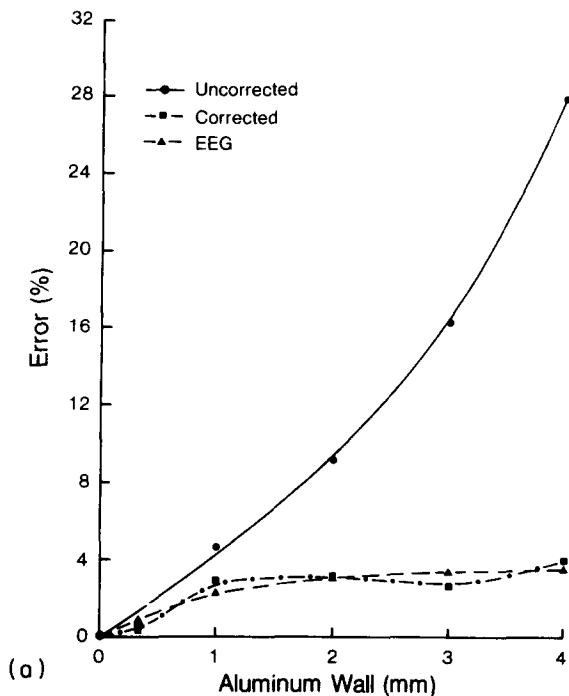


FIG. 5. Results of the phantom evaluations showing uncorrected and corrected values for the K_2HPO_4 solution in relation to the aluminum-wall thickness. The calculated curve for the EEG effect is also shown; (a) represents the values measured without the scatter collimator and (b) those with the scatter collimator.

close to the theoretical error for the EEG effect. The error due to scatter is, therefore, to a large extent removed. Without the scatter collimator in place, the optimal parameter values were $p = 1.84 \times 10^{-4}$ and $n = 51$; with the scatter collimator we obtained $p = 2.08 \times 10^{-4}$ and $n = 21$. There are several pairs of parameter values that produce similar results for the measurements with the scatter collimator mounted, but only a slight deviation is permitted for the measurements obtained without the scatter collimator.

In order to compare the above results with a correction method that assumes scatter to be a constant fraction of the incident photon flux,^{4,5} we varied the subtractive amount of scatter for the same phantom measurements to minimize the error with respect to the EEG curve (Fig. 6). The same procedure as for optimizing the p and n values was employed. Whereas the assumption of a constant fraction of scatter produces only slightly inferior results in the absence of large amounts of scattered photons (i.e., scatter collimator mounted), the new method is clearly superior if the scatter contribution is increased.

The performance of the scatter correction process was finally tested with our forearm phantom which contains a larger and a smaller aluminum cylinder (wall thicknesses: 2.24 and 1.65 mm, respectively) side by side in a Plexiglas cylinder, representing the cortical bone of radius and ulna. As this phantom is not symmetrical, the effects of the aluminum cylinders onto their respective central parts are not expected to be quite as pronounced. The difference in density of the central areas within the aluminum cylinders was negligible for the measurement with the scatter collimator mounted, and the scatter correction changed this difference

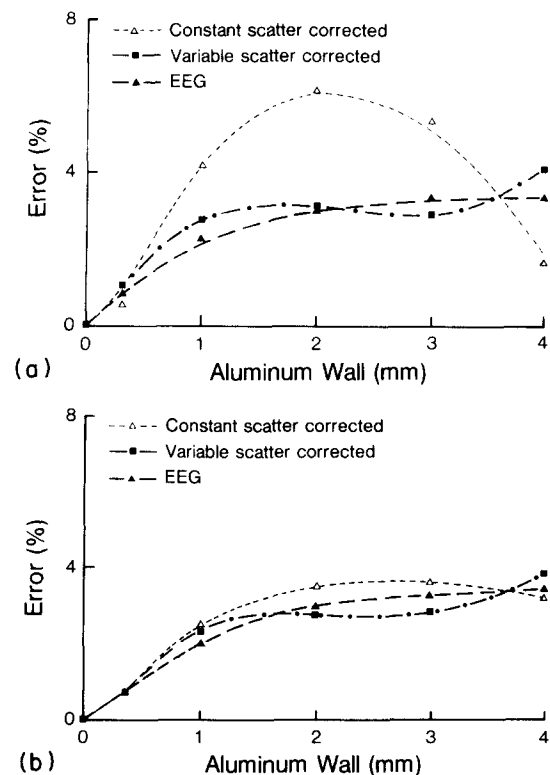


FIG. 6. Comparison of correction with constant scatter and with the new method; (a) and (b) represent the same cases as in Fig. 5.

only minimally. However, for the measurement with no scatter collimator in place, the inner area of the smaller cylinder was 3.9% lower in density than the respective area within the larger cylinder. Application of the scatter correction reduced this difference to 0.5%. The actual value of the Plexiglas within the aluminum cylinders was higher compared with the Plexiglas outside as expected because of the EEG effect.

V. DISCUSSION

The scattering-induced error in a phantom with aluminum rings of varied thicknesses is considerable. Although the greater thicknesses exaggerate the anatomical situation, this phantom was useful in developing an appropriate correction procedure. The amount of cortical bone at the distal end of the radius or tibia normally does not exceed the equivalent of 2 mm aluminum. Up to this wall thickness, the maximum remaining error due to scatter (corrected value – EEG value) is 0.61% for measurements without the scatter collimator and 0.34% for those with the scatter collimator in place. The maximum error in the same range of the aluminum wall thickness without the scatter correction applied is 6.22% and 0.71%, respectively. It was also shown with the forearm phantom that the measurements with the scatter collimator in place do not really need a software scatter correction, because the anatomical range of cortical wall thickness distorts the trabecular bone results only minimally. However, we have to keep in mind that the large distance of the detectors from the measurement object allows a very long collimation path against scatter, which is generally not available in commercial systems. The results of measuring the phantom with varied aluminum-wall thicknesses within a water-filled body phantom on a GE 8800 scanner are plotted in Fig. 7. The data were analyzed employing Cann and Genant's method¹⁴ of reference solutions. However, our correction procedure could not be applied to these data because access to the raw data was not available.

The parameter p , which was optimized for both the case without and the case with the scatter collimator in place, turned out to be very similar in both situations ($p = 1.84 \times 10^{-4}$ and $p = 2.08 \times 10^{-4}$). As mentioned previously, the two parameters p and n allow a certain combined variation for the measurements with the scatter collimator in place without changing the result. Whereas p can theoretically be varied in small increments, n has to be an odd integer number in order to keep the summation symmetrical. Consequently, the optimal p for a given n can assume only discrete values and is not a free variable anymore. Rather than using the sensitivity profile of the detectors given through the arrangement of the detector and scatter collimators (trapezoid of 27 data points base and 13 data points top) we employed equal weighting in the summation process. The optimal n of 21 corresponds well with the theoretical full width at half maximum (FWHM) of the sensitivity profile which is 20 data points.

In developing the scatter correction, we have replaced $f(\mu_s/\mu)$ with p [Eqs. (7) and (8)]. This is a material-dependent parameter, but taken as a constant in the correction

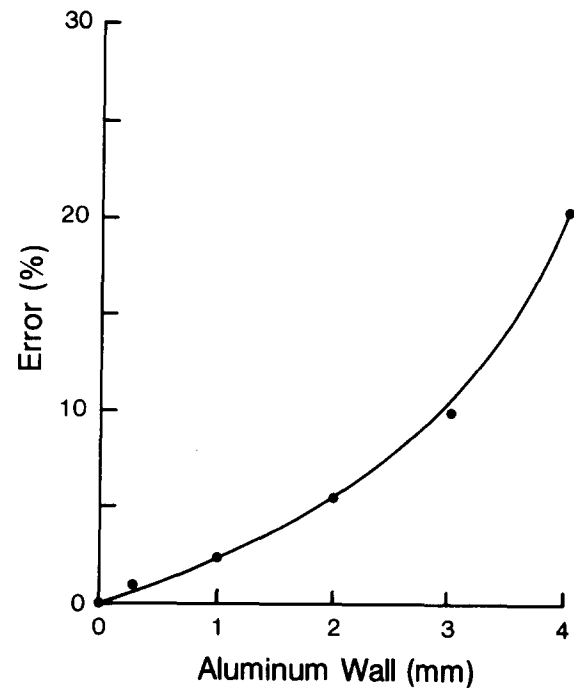


FIG. 7. Measurement on a GE 8800 CT scanner of the phantom in a water-filled tank simulating a body cross section with the spine. The CT values of the K_2HPO_4 solution were referenced to the calibration phantom usually employed for spinal bone measurements.

process, because the major amount of scatter is produced by the water in the phantom. For water, μ_s/μ has a value of 0.63. The f factor is representing the fraction of forward-scattered photons and has to be calculated separately for coherent and incoherent scattering. The combined f factor is then obtained by summing the two components after weighting them with the relative contribution of coherent and incoherent scattering. The amount of scatter sent in the forward direction can be estimated based on the tables by Hubbell *et al.*¹⁵ and can be related to the amount of scatter observed under the same solid angle if it were distributed isotropically. This forward preference amounts to 3.93 for coherent and 1.40 for incoherent scatter, and it results in 1.91 as weighted average. Based on the detector collimator of 2×5 mm, the fraction of the total 4π solid angle of a source at the center of rotation is 1.80×10^{-5} . The bead size of the isotope (1.2 mm), width of the detector collimator (2.0 mm), and translational movement (0.3 mm) result in a beamwidth of 1.5 mm (FWHM), which is equivalent to 5.2 intervals or pixels. Because the summation of the scatter count rates is performed over n intervals, the beamwidth of five intervals has to be taken into account when theoretically calculating the parameter p . The product of all the factors contributing to p yields 1.13×10^{-4} . This value is about 40% below the experimental value of 1.84×10^{-4} . Although the calculations reflect the same order of magnitude as the experiment, the simplicity of the scatter model does not take all scatter sources into account. Because of the long collimator walls, additional scatter occurs particularly in the forward direction (high- z material), and this virtually increases the collimator opening. In addition, some second- and higher-order scatter occurs, which is not accounted for in the calculations.

However, there is only a minimal amount of higher-order scatter. This was tested by placing a collimator existing only of two parallel bars in the position of the scatter collimator. The bar collimator basically removed all photons from scatter events that occurred outside the measurement plane. The measured phantom showed only slightly less density increase in the center with increasing aluminum-wall thickness than the one measured without a scatter collimator at all. Besides illustrating the good collimation of the source to the measurement plane, this experiment confirmed the assumption of the model that predominantly first degree scatter is responsible for the observed effects.

Based on the experimentally defined values for p and n we can calculate the amount of scatter of a projection beam and compare it to the measured values (Sec. II). The calculated scatter-to-primary ratio is 1.67×10^{-2} for the measurements without the scatter collimator and 5.10×10^{-3} for those with the scatter collimator. These numbers are larger by a factor of 2.9 and 69.4, respectively, as compared with the measured scatter ratios. The discrepancy can be explained by the fact that blocking off the primary photon beam for the scatter measurements also blocks off all scattered photons that arrive on the same path. The rejection of most scattered photons not in a narrow forward direction by the scatter collimator accounts for the large difference in the case of the scatter collimator in place.

The correction procedure described uses only a first approximation for estimating the number of scattered photons seen by the detectors. Despite the simplifying assumptions, which allow fast implementation of the correction procedure in the image-reconstruction algorithm, the scattering-induced error was decreased considerably. Over the range of aluminum ring thicknesses investigated, this reduction averaged 95% for the measurements without the scatter collimator, and 75% for the measurements with the scatter collima-

tor in place. The results could probably be improved by applying correction procedures of greater complexity and assuming higher-order scatter as well as actual material distribution in the measured cross section. Such a procedure would probably be of iterative type, as at least a preliminary reconstructed image is needed for estimating the material distribution. Any further improvement of accuracy of the pixel values would require simultaneous correction of the error that is caused by the EEG effect as well as of residual errors due to beam hardening.

ACKNOWLEDGMENTS

I would like to thank Dr. T. R. Overton for valuable suggestions in the preparation of this manuscript. I am indebted to the Alberta Heritage Foundation for Medical Research for financial assistance in the form of a Scholarship.

^{a)} Present address: Department of Biomedical Engineering, Wright State University, Dayton, OH 45435

¹P. C. Johns and M. Yaffe, *Med. Phys.* **9**, 231 (1982).

²G. H. Glover, *Med. Phys.* **9**, 860 (1982).

³H. Kanamori, N. Nakamori, K. Inoue, and E. Takenaka, *Phys. Med. Biol.* **30**, 239 (1985).

⁴P. M. Joseph and R. D. Spital, *Med. Phys.* **9**, 464 (1982).

⁵P. R. Moran, W. S. Y. Kwa, and S. A. G. Chenery, *Phys. Med. Biol.* **28**, 939 (1983).

⁶H. K. Genant and D. Boyd, *Invest. Radiol.* **12**, 545 (1977).

⁷P. Rügsegger, T. Hangartner, H. U. Keller, and T. Hinderling, *J. Comput. Assist. Tomogr.* **2**, 184 (1978).

⁸A. M. Laval-Jeantet, C. E. Cann, B. Roger, and P. Dallant, *J. Comput. Assist. Tomogr.* **8**, 1164 (1984).

⁹T. N. Hangartner and T. R. Overton, *J. Comput. Assist. Tomogr.* **6**, 1156 (1982).

¹⁰L. A. Shepp and B. F. Logan, *IEEE Trans. Nucl. Sci.* **NS-21**, 21 (1974).

¹¹Wm. J. Veigle, *At. Data* **5**, 51 (1973).

¹²ICRP Publ. No. 23, Pergamon, New York, (1975).

¹³P. M. Joseph and R. D. Spital, *Phys. Med. Biol.* **26**, 473 (1981).

¹⁴C. E. Cann and H. K. Genant, *J. Comput. Assist. Tomogr.* **4**, 493 (1980).

¹⁵J. H. Hubbell, W. J. Veigle, E. A. Briggs, R. T. Brown, D. T. Cromer, and R. J. Howerton, *J. Phys. Chem. Ref. Data* **4**, 471 (1975).